3. Wang Q-Y et al. *Chinese Phys. Lett.* **29** 037402 (2012)
4. Liu D et al. *Nature Commun.* **3** 931 (2012)
5. Sadovskii M V *Phys. Usp.* **51** 1201 (2008); *Usp. Fiz. Nauk* **178** 1243 (2008)
6. Ivanovskii A L *Phys. Usp.* **51** 1229 (2008); *Usp. Fiz. Nauk* **178** 1273 (2008)
7. Izyumov Yu A, Kurmaev E Z *Phys. Usp.* **51** 1261 (2008); *Usp. Fiz. Nauk* **178** 1307 (2008)
8. Ishida K, Nakai Y, Hosono H *J. Phys. Soc. Jpn.* **78** 062001 (2009)
9. Johnston D C *Adv. Phys.* **59** 803 (2010)
10. Paglione J, Greene R L *Nature Phys.* **6** 645 (2010)
11. Mazin I I *Nature* **464** 183 (2010)
12. Lumsden M D, Christianson A D *J. Phys. Condens. Matter* **22** 203203 (2010)
13. Wen H-H, Li S *Annu. Rev. Condens. Matter Phys.* **2** 121 (2011)
14. Basov D N, Chubukov A V *Nature Phys.* **7** 272 (2011)
15. Stewart G R *Rev. Mod. Phys.* **83** 1589 (2011)
16. Hirschfeld P J, Korshunov M M, Mazin I I *Rep. Prog. Phys.* **74** 124508 (2011)
17. Boeri L, Dolgov O V, Golubov A A *Phys. Rev. Lett.* **101** 026403 (2008)
18. Eschrig H, arXiv:0804.0186
19. Ning F et al. *J. Phys. Soc. Jpn.* **78** 013711 (2009)
20. Lebègue S *Phys. Rev. B* **75** 035110 (2007)
21. Singh D J, Du M-H *Phys. Rev. Lett.* **100** 237003 (2008)
22. Mazin I I et al. *Phys. Rev. Lett.* **101** 057003 (2008)
23. Graser S et al. *New J. Phys.* **11** 025016 (2009)
24. Cao C, Hirschfeld P J, Cheng H-P *Phys. Rev. B* **77** 220506(R) (2008)
25. Kordyuk A A *Low Temp. Phys.* **38** 888 (2012); *Fiz. Nizk. Temp.* **238** 1119 (2012)
26. Brouet V et al. *Phys. Rev. B* **86** 075123 (2012)
27. Berk N F, Schrieffer J R *Phys. Rev. Lett.* **17** 433 (1966)
28. Scalapino D J *J. Low Temp. Phys.* **117** 179 (1999)
29. Scalapino D J, Loh E (Jr.), Hirsch J E *Phys. Rev. B* **34** 8190(R) (1986)
30. Kontani H, Onari S *Phys. Rev. Lett.* **104** 157001 (2010)
31. Onari S, Kontani H *Phys. Rev. B* **85** 134507 (2012)
32. Castellani C, Natoli C R, Ranninger J *Phys. Rev. B* **18** 4945 (1978)
33. Oleś A M *Phys. Rev. B* **28** 327 (1983)
34. Kuroki K et al. *Phys. Rev. Lett.* **101** 087004 (2008)
35. Kemper A F et al. *New J. Phys.* **12** 073030 (2010)
36. Ikeda H *J. Phys. Soc. Jpn.* **77** 123707 (2008)
37. Ikeda H, Arita R, Kuneš J *Phys. Rev. B* **81** 054502 (2010)
38. Zhang J et al. *Phys. Rev. B* **79** 220502(R) (2009)
39. Chubukov A V, Efremov D V, Eremin I *Phys. Rev. B* **78** 134512 (2008)
40. Thomale R et al. *Phys. Rev. Lett.* **106** 187003 (2011)
41. Maiti S et al. *Phys. Rev. Lett.* **107** 147002 (2011)
42. Maiti S et al. *Phys. Rev. B* **84** 224505 (2011)
43. Maiti S, Korshunov M M, Chubukov A V *Phys. Rev. B* **85** 014511 (2012)
44. Mazin I I *Phys. Rev. B* **84** 024529 (2011)
45. Korshunov M M et al. *J. Supercond. Novel Magn.* **26** 2873 (2013)
46. Khodas M, Chubukov A V *Phys. Rev. Lett.* **108** 247003 (2012)
47. Kreisel A et al. *Phys. Rev. B* **88** 094522 (2013)
48. Korshunov M M, Eremin I *Phys. Rev. B* **78** 140509(R) (2008)
49. Maier T A, Scalapino D J *Phys. Rev. B* **78** 020514(R) (2008)
50. Inosov D S et al. *Nature Phys.* **6** 178 (2010)
51. Christianson A D et al. *Nature* **456** 930 (2008)
52. Lumsden M D et al. *Phys. Rev. Lett.* **102** 107005 (2009)
53. Christianson A D et al. *Phys. Rev. Lett.* **103** 087002 (2009)
54. Park J T et al. *Phys. Rev. B* **82** 134503 (2010)
55. Argyriou D N et al. *Phys. Rev. B* **81** 220503(R) (2010)
56. Castellan J-P et al. *Phys. Rev. Lett.* **107** 177003 (2011)
57. Qiu Y et al. *Phys. Rev. Lett.* **103** 067008 (2009)
58. Babkevich P et al. *J. Phys. Condens. Matter* **22** 142202 (2010)
59. Onari S, Kontani H, Sato M *Phys. Rev. B* **81** 060504(R) (2010)
60. Onari S, Kontani H *Phys. Rev. B* **84** 144518 (2011)

PACS numbers: **74.25.–q**, **74.45.+c**, 74.62.Dh, 74.70.Xa
DOI: 10.3367/UFNe.0184.201408i.0888

Andreev spectroscopy of iron-based superconductors: temperature dependence of the order parameters and scaling of $\Delta_{L,S}$ with T_c

T E Kuzmicheva, S A Kuzmichev, M G Mikheev, Ya G Ponomarev, S N Tchesnokov, V M Pudalov, E P Khlybov, N D Zhigadlo

1. Introduction

The unexpected discovery in 2006 [1] of the first layered Fe-based high-temperature superconductor (HTSC), LnOFePn (where Ln is lanthanide, Pn is pnictide; hereafter referred to as 1111), becomes a key issue in modern solid-state physics. Since 2008, the class of iron-based superconductors has greatly expanded: several families of iron pnictides and chalcogenides have been synthesized [2–4]. The crystal structure of oxypnictides is reminiscent of that of cuprates and is, in fact, a stack of superconducting Fe–As layers alternating along the *c*-direction with spacers, nonsuperconducting oxide blocks, Ln–O. In spite of the pronounced layered structure and anisotropic physical properties, the electron subsystem in Fe-based superconductors is less quasi-two-dimensional than that in cuprate HTSC, because the height of the Fe–As blocks exceeds the thickness of the CuO_2 planes, whereas the distance between superconducting blocks in iron-based superconductors is significantly shorter than that in cuprates. This seems to be a reason [5] why the critical temperature of Fe-based superconductors, though being as high as $T_c \approx 57.5$ K [6], still does not reach the cuprate one.

Superconductivity in novel materials emerges with the suppression of a spin-density-wave ground state under doping of the superconducting Fe–As layers or under external pressure [7]. The key distinction from cuprates, however, lies in the multiband nature of newly discovered superconductivity in iron-based materials. Band structure calculations have shown (for a review, see Ref. [8]) the coexistence of the electron and the hole quasi-two-dimensional bands in these com-

T E Kuzmicheva. Lebedev Physical Institute, Russian Academy of Sciences, Moscow; Lomonosov Moscow State University, Faculty of Physics, Russian Federation
E-mail: kute@sci.lebedev.ru
S A Kuzmichev, M G Mikheev, Ya G Ponomarev, S N Tchesnokov. Lomonosov Moscow State University, Faculty of Physics Russian Federation
V M Pudalov. Lebedev Physical Institute, Russian Academy of Sciences, Moscow, Russian Federation; Moscow Institute of Physics and Technology (State University), Dolgoprudnyi, Moscow region, Russian Federation
E P Khlybov. Vereshchagin Institute of High Pressure Physics, Russian Academy of Sciences, Troitsk, Moscow region, Russian Federation; International Laboratory for High Magnetic Fields and Low Temperatures, Wroclaw, Poland
N D Zhigadlo. Laboratory for Solid State Physics, ETH Zurich, Zurich, Switzerland

Uspekhi Fizicheskikh Nauk **184** (8) 888 – 897 (2014)
DOI: 10.3367/UFNr.0184.201408i.0888
Translated by T E Kuzmicheva; edited by A Radzig

pounds, whereas the Fermi surfaces consist of cylinders slightly warped along the *c*-direction (near the Γ and M points), where several superconducting condensates could form.

Contrary to the observation of the strong isotope effect [9], an early theoretical study [10] revealed that the high-temperature superconductivity in Fe-based compounds could not be based on the electron–phonon interaction solely. Although this interaction plays an important role, it is incapable [10] of explaining the observable values of T_c in the framework of the Eliashberg theory [11]. Taking into account the nesting of the Fermi surface sheets along the Γ–M-direction, the vicinity of the antiferromagnetic state [12, 13], and the appearance of the experimentally detected [14] peak of dynamic spin susceptibility ('magnetic resonance'), Mazin et al. [12] suggested a theoretical description of the mechanism of superconductivity in iron pnictides and chalcogenides based on a sign-changing (in different bands) order parameter — the so-called $s^{\pm}$-model. The simplest initial model considers two isotropic order parameters (in the electron and the hole bands, respectively), which have equal amplitudes but are in antiphase (i.e., have opposite signs). The strong interband interaction mediated by spin fluctuations along the Γ–M-direction plays the key role in this model, whereas the intraband electron–phonon coupling is an order of magnitude weaker. Later on, the initial model was found to be inadequate, in particular, because of its instability with respect to the impurity scattering [15–21], and the $s^{\pm}$-model has been extended [22].

According to the results of calculations in the framework of the $s^{\pm}$-system, the magnetic resonance energy should not exceed the width of the larger superconducting gap: $E_{res} \leqslant 2\Delta_L$ [13, 14]. However, the experimentally observed (see paper [16] and references cited therein) susceptibility peak is rather smeared, whereas its position does not always satisfy the resonance condition [15, 16]. Moreover, the most recent study for cuprates [23] showed that similar 'magnetic resonance' is determined by the superconductor itself, while its energy coincides with 2Δ. An alternative theory of the two-gap state of Fe-containing superconductors is based on the coupling through orbital fluctuations [16]. This model is capable of describing such superconductivity within the framework of the constant-sign order parameter (s^{++} type of symmetry).

Nevertheless, the two competing theories [12, 16] do not deny the importance of the electron–phonon coupling underlying the intraband interaction within each of the superconducting condensates. On the other hand, as was shown in Ref. [24], the Allen–Dynes formula fails to provide such high-T_c values as experimentally obtained. This led the authors of Ref. [24] to a conclusion on the significance of nonphonon mechanisms of Cooper pairing in such compounds (including LnOFePn). Moreover, the T_c variation for various Fe-based superconductors was shown to be related to the variation of the density of states at the Fermi level. Within a single family of Fe-based superconductors, such T_c variation can be caused by the modification of the chemical composition of spacers. Similar remote doping (δ-doping) of superconducting blocks is successfully practiced for cuprates.

This work is concerned with both an experimental verification of the aforementioned issue and a comparison of values of the relative parameter, namely the characteristic ratio of the Bardeen–Cooper–Schrieffer (BCS) theory, $2\Delta_L/(k_B T_c)$, that evidences the strength of electron–boson coupling in LnOFeAs compounds (1111 family) with various T_c.

2. Review of the experimental research

Despite the fact that iron-based superconductivity was discovered eight years ago, many of its aspects still remain obscure. There is no common agreement on such issues as the mechanism of superconductivity or the number and the symmetry of superconducting gaps. The experimentally determined superconducting energy gaps and the magnetic resonance energy, the key parameters of iron-based compounds, are rather contradictory. Experimentalists face a number of obstacles. The majority of traditional techniques applied to determine the superconducting gap values (specific heat, London penetration depth, and nuclear magnetic resonance (NMR)) include processing of the experimental data on the basis of theoretical models. These models usually neglect the anisotropy of the transport and superconducting properties, thus giving volume-averaged energy parameters. In particular, the synthesis of the large-sized oxypnictide single crystals has still not been developed [see paper [25] and references cited therein]; therefore, their properties are measured mostly with polycrystalline samples. All this is a plausible reason for the low resolution of the nonlocal techniques, whereas the measured parameters often appear to be reduced.

Indeed, the temperature dependence of the London penetration depth measurements [26–28] reveals only a single superconducting gap with $2\Delta/(k_B T_c) \leqslant 3.52$, where the maximal ratio $2\Delta/(k_B T_c) \approx 3.4$ was obtained for single crystals [27]. Similar BCS ratios were found in optical studies [29], as well as conducting research into specific heat [30], and NMR [31]. Two distinct superconducting gaps with rather high BCS ratios, $2\Delta_L/(k_B T_c) \approx 7-8$ and $2\Delta_S/(k_B T_c) \approx 2-3$, have been resolved by NMR [32, 33], and the authors do not exclude a possible d-wave symmetry.

Widely used local techniques, such as point-contact spectroscopy, scanning tunneling microscopy (STM), and angle-resolved photoemission spectroscopy (ARPES), are based on probing surface properties of the sample; hence, the data become strongly affected by the surface defects. In so-called 1111 oxypnictides, which are easily cleaved along the *ab*-planes (between the Fe–As and Ln–O layers) due to substantial anisotropy, their cleaved surface appears to be charged [34]. A similar effect is absent only for the (Li, Na)FeAs family (so-called 111 system), which could make this system a prime subject for surface techniques. However, there are additional fundamental obstacles: the alkali-metal atoms make the 111 superconductors extremely reactive, and, therefore, fast-degrading (particularly in the presence of oxygen or water vapor).

To date, there are no ARPES data resolving both superconducting gaps. The ARPES studies certainly resolve clearly the large gap opening at the hole cylinder near the Γ-point of the Fermi surface, although its anisotropy is ambiguous. As was demonstrated in Ref. [35] for Nd-1111 single crystals, the large gap has no nodes in the *k*-space, whereas its BCS ratio $2\Delta/(k_B T_c) \approx 6.6$, being typical for a strong electron–boson coupling, is close to the value estimated in our studies. At the same time, the data for La-1111 polycrystallines [36] are in agreement with both the d- and s-wave models, while the BCS ratio is lower: $2\Delta/(k_B T_c) \sim 3.6$ in the s-wave

model approximation, and $2\Delta/(k_B T_c) \sim 4.1$ in the case of d-symmetry of the order parameter.

The dynamic conductance of the tunnel NIS contacts (N is a normal metal, S is a superconductor, I is an insulator) was studied in a number of works by STM [37–41]. These studies have resolved the only superconducting gap with $2\Delta/(k_B T_c) = 3.5-4$. In Refs [42, 43], NIS spectra exhibiting peculiarities caused by two isotropic gaps, Δ_L and Δ_S, were obtained with Nd-1111 polycrystalline samples. The BCS ratio for the large gap was estimated as $2\Delta_L/(k_B T_c) = 6.2 \pm 0.7$, which agrees with that obtained by NS spectroscopy [44], and the results presented here. The presence of the reproducible fine structure in the spectra was also demonstrated in Ref. [43]. This structure corresponds well to the calculated Eliashberg function $\alpha^2 F(\omega)$ and the phonon density of states found experimentally in Ref. [45]; therefore, it is believed to have a phonon nature [43]. Moreover, the critical temperature $T_c^{\text{theory}} = 48.8$ K estimated from $\alpha^2 F(\omega)$ calculations using the single-gap s-wave model was found to be similar to the real critical temperature of the sample $T_c^{\text{sample}} \approx 51$ K, thus confirming the conclusion of Ref. [43] on the intraband strong electron–phonon coupling.

The divergence of the experimental results on the superconducting gap values by more than a factor of six for the spread of the $2\Delta_L/(k_B T_c)$ values: $2\Delta_L/(k_B T_c) = 3.5-22.3$ and on the number of the gaps observed is impressive (see reviews [46, 47]). This divergence is intrinsic to the most popular tunneling technique: the point contact spectroscopy of NS junctions. Unfortunately, in 1111 polycrystalline samples, the technique faces such problems as a degraded surface or inability to use silver paste for the point contact. The dynamic conductance spectra obtained in Refs [48, 49] with La-1111 and Sm-1111 contain pronounced maxima related to the small gap, whereas the large gap peculiarities are faded. The strong asymmetry of the NS spectra and the necessity of seven parameter fitting (for a two-gap superconductor) surely obstruct the data interpretation and lead to the data spread. For example, the BCS ratio [48] for Sm-1111 with various dopant concentrations and the corresponding range $13.5 \leqslant T_c \leqslant 52$ K varied within the range of 8–22 for the large gap, and 1.9–6.8 for the small gap. Such great variations could be caused only by changing the coupling mechanism as the doping level was varied.

This assumption seems highly improbable, especially for the 1111 family. The gap temperature dependences measured in Ref. [49] for La-1111 and Sm-1111 turned out very dissimilar. For Sm-1111 samples, a BCS-like 'closing' of both gaps was observed [49]. At the same time, for La-1111, the large gap vanished abruptly already at $2/3T_c$, whereas the small gap deviated from the BCS-like curve and linearly tended to zero at T_c [49]. Such behavior of the gaps does not agree with the Moskalenko and Suhl system of gap equations [50–52] for two-gap superconductivity and was not confirmed in any subsequent work with Fe-based superconductors. The authors of Ref. [49] suggest no explanation for that gap behavior either, referring to it as an 'artefact'. Summarizing some experimental data in Ref. [49], this group of researchers presented the dependences of the BCS ratios (for the large and the small gaps) on the critical temperature for various iron-based superconductors. According to Ref. [49], $2\Delta_{L,S}/(k_B T_c)$ increases as T_c decreases, dramatically rising as $T_c \to 10$ K, which seems unconvincing to us both from common sense arguments and because it is unjustified by experiment.

3. Experimental details

The overview presented in Section 2 demonstrated the necessity of *direct* highly precise experimental probing of the superconducting gaps and their temperature dependences to clarify features and the mechanism of superconductivity in iron-based compounds. To address this issue, we applied Andreev spectroscopy [53, 54] of the *symmetric* SnS contacts. With such a contact, when its diameter a is less than the quasiparticle mean free path l [55], an effect of multiple Andreev reflections from both NS boundaries occurs. In this case, the current–voltage characteristic (CVC) shows a linear region with an excess current at low bias ('foot') and a series of peculiarities at bias voltages

$$V_n = \frac{2\Delta}{en}, \quad n = 1, 2, \ldots, \tag{1}$$

referred to as the subharmonic gap structure (SGS) [56–59]. For a high-transparent contact, the dynamic conductance spectrum $dI(V)/dV$ demonstrates a series of *minima*. For a two-gap superconductor, two such SGSs corresponding to both gaps should appear [60, 61]. A finite l/a ratio at low biases V decreases the probability of ballistic transport through the SnS interface for a quasiparticle, which causes fading of the Andreev reflection peculiarities with increasing the harmonic number n. When V decreases (and n increases) to satisfy $an \approx l$, the excess current saturates. As bias tends further to zero, the current also decreases, elucidating the linearity of the 'foot' in the CVC.

In our studies, we employed the *break-junction* technique [62] based on the formation of twin touching cryogenic clefts in the bulk of the sample, which are separated by a weak link (the so-called ScS contact, where c is the constriction). The sample made as a thin rectangular plate of about $3 \times 1.5 \times 0.2$ mm^3 was mounted on a springy holder using a standard four-terminal connection. To fix the sample, we used liquid pads of In–Ga alloy at its corners. Then the sample holder was cooled to $T = 4.2$ K and deformed gently enough to generate a microcrack separating the sample into two superconducting banks. The $I(V)$ and $dI(V)/dV$ characteristics of our break-junctions in Fe-based superconductors [63–75] are typical for the high-transparency Andreev regime with ballistic transport (see Figs 2b and 5 from Ref. [57], and Fig. 4 from Ref. [59]).

The number of grains cleaved during the formation of the cryogenic cleft is known to be dependent on the $P_{\text{grains}}/P_{\text{layers}}$ ratio (P_{grains} is the intergrain solidity and P_{layers} is the interlayer solidity). Therefore, one can expect a high ratio of the cleaved-to-uncleaved crystallites along the microcrack for annealed polycrystalline samples. Simple calculations showed that $P_{\text{grains}}/P_{\text{layers}} = 1.1$ is sufficient to expect the formation of about 6% of the cleaved grains, whereas $P_{\text{grains}}/P_{\text{layers}} = 2.5$ would cause the cleavage of every second crystallite. The latter provides successful application of the break-junction technique for both single- and polycrystalline samples of layered compounds [71].

Due to the pronounced layered structure of the iron-based superconductors, the microcrack passes along the *ab*-planes and forms steps and terraces on the cryogenic clefts. The height of such steps is obviously a multiple of the c lattice parameter. The steps and terraces can be realized not only as single ScS contacts, but as array structures of the S–c–S–c–...–S type. For Fe-based superconductors, the Fe–As blocks act like S, whereas Ln–O spacers act like weak

links. Obviously, the array contact is electrically equivalent to a sequence of identical ScS contacts. Therefore, the bias voltage for any peculiarities (caused by the bulk properties of the sample) in the CVC and the dynamic conductance should be N times larger (where N is the number of junctions in the stack) for an array contact than that of a single ScS contact. Such array contacts were first observed on cuprates [76–79], and then on other layered superconductors [67–72, 74, 75]. In the Andreev mode (i.e., when the weak link formally acts as a normal metal), such arrays demonstrate the intrinsic multiple Andreev reflections effect (IMARE) [78], similar to the intrinsic Josephson effect [76, 78, 80]. Therefore, the value of a gap may be determined using the formula $V_n = 2\Delta N/(en)$.

Were one trying to attribute the observed S–c–S–c–...–S contacts in break-junction experiments to the formation of a sequence of crystallites touched via intergrain boundaries (rather than to bulk effects on natural stack structures), the result would not stand up to criticism. In the former case, due to the inequality of the intergrain boundaries, the position of the main gap peculiarities would be *accidental* rather than a multiple of $2\Delta/e$. Also, the shape and the fine structure of peculiarities in dynamic conductance spectra *would be irreproducible* under a mechanical readjustment of the contact. Moreover, increasing the number N of consequently connected grains (having different resistance in the normal state) along with the number of nonequivalent intergrain boundaries would cause dramatic smearing of peculiarities in the dI/dV spectrum. In our studies, however, the opposite picture is observed: when N increases, the spectrum quality improves, whereas the position and the shape of SGS peculiarities are *well-reproduced* under scaling of the bias axis by natural N. Furthermore, we observe a similar tendency for *single crystals* of various superconductors.

Summarizing the above, we conclude that there are a number of advantages of the employed break-junction technique:

(a) the presence of clean cryogenic clefts in the bulk of the sample: under microcrack formation, the superconducting banks can precisely slide on top of each other, along the *ab*-planes. The microcrack is not opened, preventing degradation of the surface;

(b) the break-junction provides local probing of the superconducting parameters (within a contact area about several nm in diameter);

(c) the applicability for both single crystals and polycrystalline samples of layered compounds. In particular, in Ref. [71] we showed the average diameter of the break-junction contact, 10–30 nm, to be by several orders of magnitude smaller than both the crystallite size and typical terrace width in the samples under study;

(d) the capability of probing several dozen single and array contacts on cryogenic clefts of one and the same sample using a mechanical readjustment; this improves data statistics, and enables reaching a conclusion on reproducibility of experimental data and the nanoscale homogeneity of the samples. The latter ability of the break-junction technique is similar to that of STM;

(e) the break-junction technique prevents the contact point from overheating due to remote current leads (a true four-point connection);

(f) the realization of both experimental techniques with iron-based superconductors, Andreev spectroscopy, and intrinsic Andreev spectroscopy. The latter being implemented to high-quality natural array contacts (nearly unaffected by overheating) guarantees measurements of the bulk superconducting gap values. A contribution of any surface defects to the dynamic conductance is reduced in such arrays by a factor of N; it also implies an N-fold increased precision in determining the superconducting parameters [71].

Summarizing, we note that the intrinsic Andreev spectroscopy realized by the break-junction technique is the only known tool for *local* probing of the *bulk* (nonreduced) superconducting order parameters. With this technique, the gap magnitudes can be determined directly from dynamic conductance of the SnS contacts, up to T_c [56, 57, 59] with no need to fit the experimental spectra with seven parameters.

4. Sample characterization

We utilized polycrystalline samples of oxypnictides based on different lanthanides, and both single- and polycrystalline FeSe samples. Typical temperature dependences of resistance near the superconducting transition are plotted in Fig. 1. Nearly optimal $GdO_{1-x}F_xFeAs$ samples with nominal fluorine concentrations of $0.09 \leqslant x \leqslant 0.21$ and bulk critical temperatures $T_c^{bulk} = 46-53$ K, and $GdO_{0.88}FeAs$ (circles in Fig. 1) with $T_c^{bulk} \approx 50$ K have been produced by high-pressure synthesis detailed in Refs [66, 81]. $CeO_{0.88}F_{0.12}FeAs$ samples (up triangles in Fig. 1) with $T_c^{bulk} \approx 41$ K were synthesized similarly. $Sm_{1-x}Th_xOFeAs$ samples (down triangles and squares in Fig. 1) with the range of Th doping of $0.15 \leqslant x \leqslant 0.3$ had critical temperatures $T_c^{bulk} = 40-52.5$ K, respectively; their synthesis and characterization were detailed in paper [82]. $LaO_{0.9}F_{0.1}FeAs$ samples (rhombs in Fig. 1) had the lowest critical temperature among the oxypnictides under consideration: $T_c^{bulk} = 21-29$ K [63,

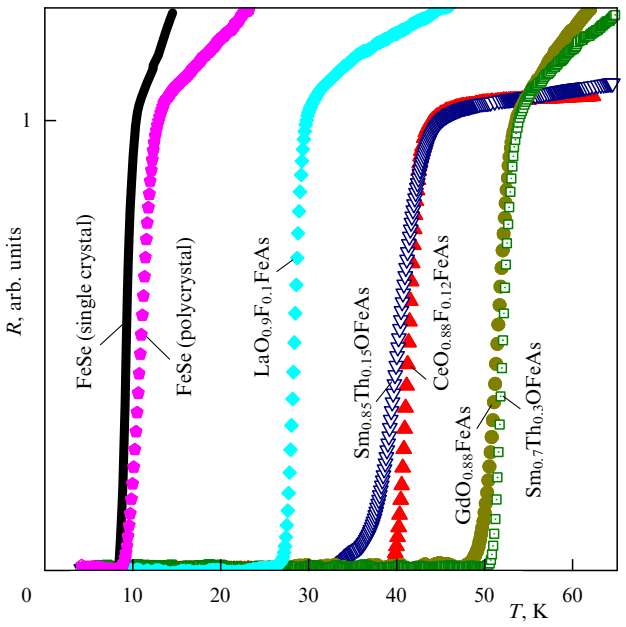

Figure 1. Normalized temperature dependences of resistance in the vicinity of the superconducting transition for various Fe-based superconductors: FeSe single crystals (solid line) with a bulk critical temperature $T_c^{bulk} \approx 9.5$ K, and polycrystals of FeSe (pentagons) with $T_c^{bulk} \approx 11$ K, $LaO_{0.9}F_{0.1}FeAs$ (rhombs) with $T_c^{bulk} \approx 28$ K, $Sm_{0.85}Th_{0.15}OFeAs$ and $Sm_{0.7}Th_{0.3}OFeAs$ (down triangles and squares) with $T_c^{bulk} \approx 40$ and 52 K, respectively, $CeO_{0.88}F_{0.12}FeAs$ (up triangles) with $T_c^{bulk} \approx 41$ K, and $GdO_{0.88}FeAs$ (circles) with $T_c^{bulk} \approx 51.5$ K.

83]. The bulk critical temperature of FeSe single crystals (solid line) was $T_c^{bulk} \approx 10$ K [73], and of polycrystalline samples (pentagons in Fig. 1) was $T_c^{bulk} \approx 11$ K [64, 70]. All the T_c^{bulk} were determined as the maximum of $dR(T)/dT$.

5. Experimental results

Figure 2 shows the dynamic conductance spectrum of single SnS contact (upper curve) and the normalized spectra of Andreev arrays (with $N = 2$, 6, 9, and 8). The contacts were formed in several optimally doped $GdO_{1-x}F_xFeAs$ and $GdO_{0.88}FeAs$ samples [65, 66, 71] with critical temperatures $T_c = 46-50$ K. The spectra demonstrate pronounced peculiarities involving the most intensive minima at $V_{L1} \approx 22$ mV and $V_{L2} \approx 11$ mV (their positions are marked in Fig. 2 by gray areas covering a 10% range of uncertainty and itemized under n_L labels), as well as peculiarities at $V_{L3} \approx 7.3$ mV (labelled as $n_L = 3$). According to Eqn (1) for the subharmonic gap structure (SGS), these peculiarities are interpreted as the first, second, and third Andreev minima for the large gap $\Delta_L \approx 11$ meV. The next peculiarity located at lower bias $V \approx 5.5$ mV is much more intensive than the third minimum for Δ_L and, hence, cannot be attributed to the fourth Andreev peculiarity of the large-gap SGS. Therefore, this minimum starts a new SGS consisting of peculiarities at $V_{S1} \approx 5.5$ mV and $V_{S2} \approx 2.7$ mV (marked by dashed areas depicting the uncertainty range, and by n_S labels in Fig. 2), and determining the small gap value $\Delta_S = 2.7 \pm 0.3$ meV.

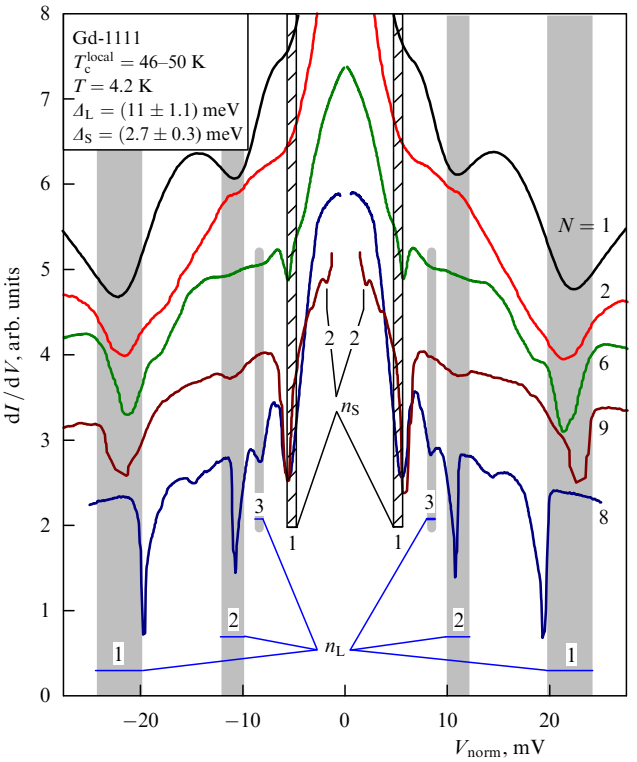

Figure 2. (Color online) Dynamic conductance spectra for SnS-Andreev arrays (four bottom lines) with the number of junctions in the stack $N = 2$, 6, 9, and 8, respectively. The curves were normalized to the spectrum for a single SnS contact (top line, $N = 1$). The SnS contacts were obtained in various GdO(F)FeAs samples with bulk critical temperatures $T_c = 46-50$ K. The positions of subharmonic gap structure minima for the large gap $\Delta_L = 11.0 \pm 1.1$ meV are marked by gray areas and itemized under n_L, and for the small gap $\Delta_S = 2.7 \pm 0.3$ meV by hatched areas, arrows, and respective n_S. The area widths depict the range of gap values.

In our studies of Fe-based superconductors, we have obtained several hundred various single and array Andreev contacts; in the corresponding spectra, two distinct SGSs have been observed [63–75]. The positions of the peculiarities for both the large and the small gaps coincided after the scaling of array contact spectra to those of the single contact (i.e., the scaling of the bias axis to an *integer*).

These results mean that on ScS contacts we observed reproducibly the multiple Andreev reflections effect (MARE) and the intrinsic multiple Andreev reflections effect (IMARE). Moreover, SnS-Andreev and intrinsic Andreev spectroscopies gave similar results. Since the array contacts are a part of the natural structure of iron-based superconductors, we conclude on the Andreev type transport along the *c*-direction in these compounds.

The high quality of the break junctions enables us to resolve the fine structure of the Andreev reflection peculiarities. It is worth noting the reproducibility of the slightly asymmetric shape of the first minima for the large gap (see Fig. 2): when bias decreases, the dynamic conductance first falls abruptly, and then smoothly rises. The latter could be a sign of a 20–30% anisotropy of Δ_L in the *k*-space (i.e., an extended s-type symmetry of the order parameter) [71]. Reaching an analogous conclusion about the Δ_S anisotropy is impossible due to the location of the small gap SGS in the increased dynamic conductance region ('foot' of the large gap) which impedes an interpretation of the Δ_S Andreev minima shape. The significant amplitude of the first SGS minima for both Δ_L and Δ_S gaps allows us to conclude indirectly that there is an absence of nodes in the *k*- direction dependence of the superconducting order parameters.

Figure 3 depicts the temperature variation of the large and the small gap SGSs in the normalized (to the integer N) $dI(V)/dV$ spectrum of an array Andreev contact. The corresponding spectrum measured at $T = 4.2$ K in a $GdO_{0.88}FeAs$ sample is presented in Fig. 2 (the third curve from the top). The spectra were shifted along the vertical scale in order of increasing temperature for clearness. The strong smearing of $n_L = 3$ and $n_S = 2$ minima could be caused by the relatively large contact diameter comparable to the mean free path. Nevertheless, the main gap peculiarities (marked as $n_L = 1$ and $n_S = 1$ in Fig. 3) are clearly seen up to T_c, thus allowing us to obtain the temperature dependences of the large and the small gaps just using the formula $2\Delta_{L,S}(T) = eV_{nL,S}(T)$ *en* with no fitting procedure.

Notably, the asymmetry of minima is invariable regardless of T. With increasing temperature, these minima shift towards the low biases, and at $T = T_c^{local} \approx 50$ K the dynamic conductance becomes linear. This implies the contact area (about 10–30 nm in diameter) transition to the normal state. The local critical temperature of the contact can differ from the bulk one T_c^{bulk} determined by nonlocal techniques, such as resistive measurements (see Fig. 1). Given that T_c^{local} of the contact has been determined, one can precisely calculate the BCS ratio: $2\Delta_L/(k_B T_c^{local}) \approx 5.2 \gg 3.52$ for this contact, and $2\Delta_S/(k_B T_c^{local}) \approx 1.3 \ll 3.52$.

Similar measurements of the Andreev spectra within the range $4.2 \text{ K} \leqslant T \leqslant T_c^{local}$ give the temperature dependences of both gaps in various iron-based superconductors. As an example, $\Delta_L(T)$ (solid symbols) and $\Delta_S(T)$ (open symbols) for Sm-based (triangles and squares) and Gd-based (circles) oxypnictides [69–74] are presented in Fig. 4. First, it is obvious that the large and small gaps behave distinctly with increasing temperature. The large gap dependence $\Delta_L(T)$, in

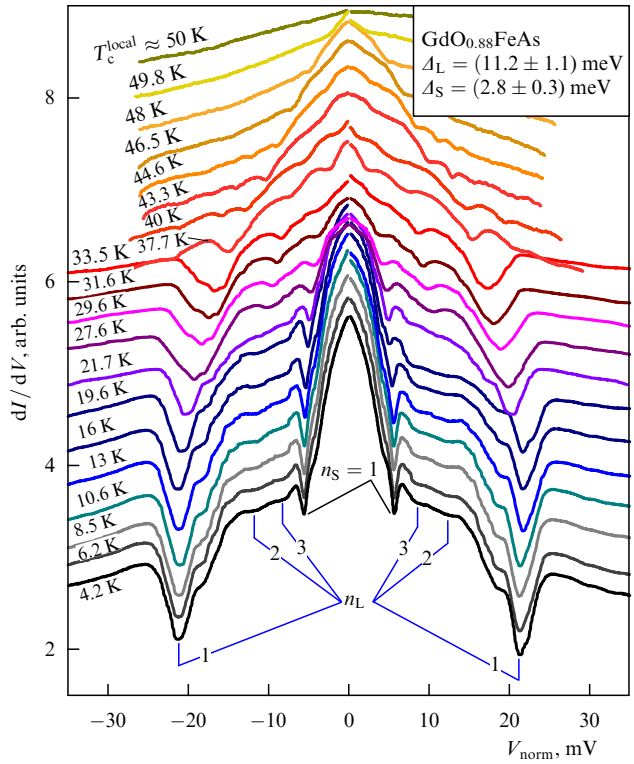

Figure 3. (Color online) Dynamic conductance of the SnS contact in a $GdO_{0.88}FeAs$ sample measured within the temperature range 4.2 K $\leqslant T \leqslant T_c^{local}$. Local critical temperature of the contact is $T_c^{local} \approx 50$ K. The spectra were shifted vertically for clearness. Andreev minima positions (at $T = 4.2$ K) for the large gap are itemized under n_L numbers, and for the small gap under $n_S = 1$.

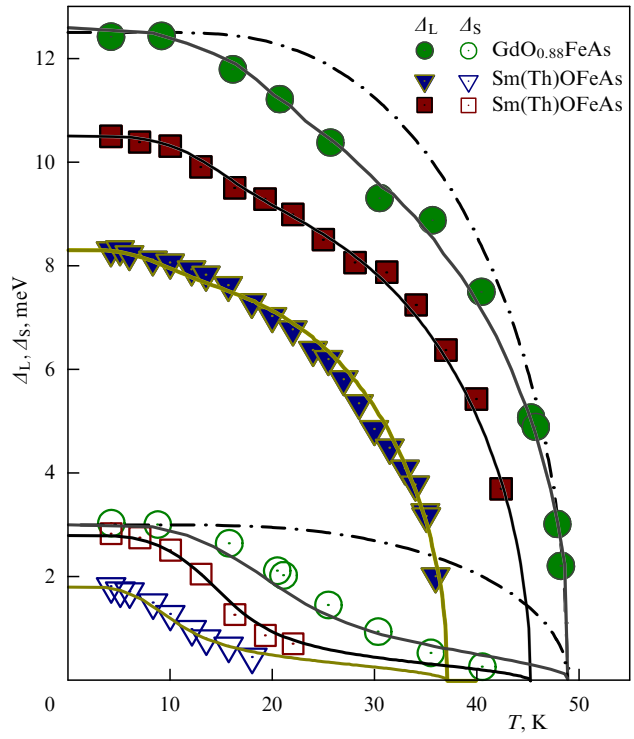

Figure 4. Temperature dependences for the large gap (solid symbols) and the small gap (open symbols) for $GdO_{0.88}FeAs$ (circles) with $T_c^{local} \approx 49$ K, and Sm(Th)OFeAs with $T_c^{local} \approx 45$ K (squares) and with $T_c^{local} \approx 37$ K (triangles). Theoretical BCS-like functions in the framework of the single-gap model (dashed–dotted lines) and two-gap model (solid lines) are presented for comparison.

general, resembles the standard BCS type (dashed–dotted lines in Fig. 4), but slightly sags due to interband interaction with the second condensate. The small gap $\Delta_S(T)$ deviates significantly from the BCS-like curve: at temperatures of about $T \sim T_c^{local}/3$, the small gap lowers abruptly, and then tends smoothly to zero at the local critical temperature. This demonstrates that the superconductivity vanishes simultaneously in both condensates at the common critical temperature T_c^{local}.

The different temperature behaviors of the large and small gaps, their discrepancy with the standard BCS-like function, and the reproducibility of the $\Delta(T)$ curves (not only for the various contacts in the same sample, but even for contacts fabricated in various compounds of the 1111 family) manifest the two-gap superconducting state (see Fig. 4), meaning that the peculiarities in SnS spectra are related to the distinct SGS and, therefore, describe the properties of different condensates. Moreover, in accordance with our findings, the gap temperature dependences look similarly for iron-based superconductors of various families (see Fig. 4, and Refs [64, 67–70, 72, 74, 75]).

To analyze the measured temperature dependences, we fitted them using a two-gap system of equations by Moskalenko and Suhl [50, 52] with a renormalized BCS integral (shown by the solid lines in Fig. 4). This system involves a set of four electron–boson interaction constants $\lambda_{ij} = V_{ij}N_j$, where V_{ij} are the matrix elements of k-space interaction between the ith and jth bands, and N_j is the normal density of states at the Fermi level of the jth band. Figure 4 demonstrates a good correspondence of the theoretical curves to the experimental data, thus showing that the two-gap BCS-like model is sufficient to describe properties of the Fe-based superconductors studied.

Therefore, the experimentally examined deviation of $\Delta_L(T)$ and $\Delta_S(T)$ from single-band dependences could be caused by a k-space proximity effect [84] between two condensates due to nonzero interband coupling. The fitting of the measured gap temperature dependences enables us to compare the strength of interband and intraband interactions of the condensates for various members of the 1111 family.

6. Discussion

The dependences of the large (solid symbols) and small (open symbols) gaps on T_c for the studied iron-based superconductors, such as Gd-1111, Sm-1111, Ce-1111, La-1111, and FeSe, are presented in Fig. 5. The critical temperatures of these compounds cover almost the whole range up to $T_c = 53$ K accessible for the 1111 family. The data related to the contacts with known T_c^{local} are depicted by the large symbols. For contacts with the spectra measured only at $T = 4.2$ K, we made use of the T_c^{bulk} (corresponding data are shown by the small symbols). As expected, the data points related to T_c^{bulk} appear to lie lower than those related to T_c^{local}, since, in general, $T_c^{bulk} > T_c^{local}$. This fact evidences the necessity of using exactly local superconducting parameters for the correct estimation of $2\Delta_{L,S}/(k_B T_c)$. The use of bulk values makes doubtful any conclusions on whether the coupling mechanism is constant or mutable under variations of electron doping for both the 1111-family compounds and other superconductors.

Our data (see Fig. 5) indicate that the two gaps are directly proportional to the critical temperature with good accuracy within the range $9 \leqslant T_c \leqslant 53$ K. The observed scaling with T_c means that the ratio of the magnitudes of the large and small

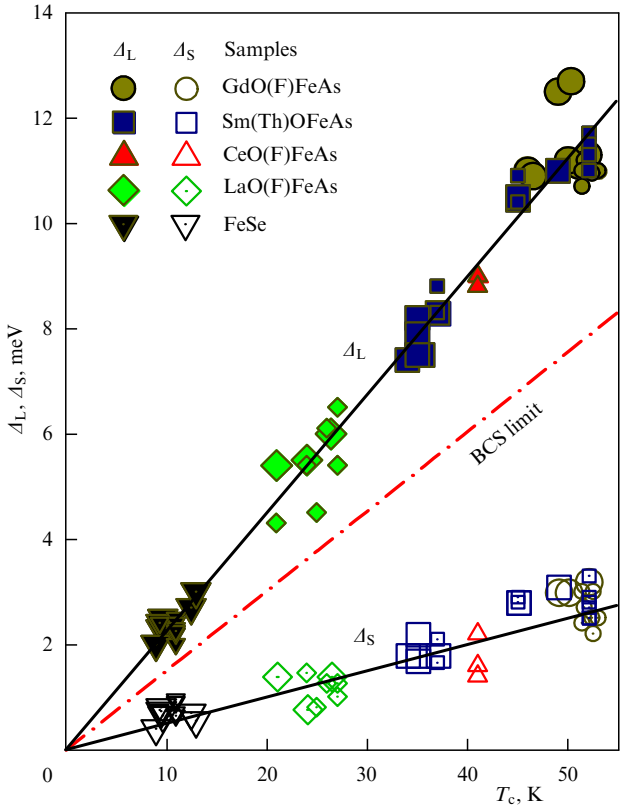

Figure 5. Dependence of the large gap (solid symbols) and small gap (open symbols) on the critical temperature for Gd-1111 (circles), Sm-1111 (squares), Ce-1111 (up triangles), La-1111 (rhombs), and FeSe (down triangles). Large symbols depict the data corresponding to T_c^{local}; small symbols show data corresponding to T_c^{bulk}. Solid guidelines are shown for clearness; the BCS limit is marked by the dashed–dotted line.

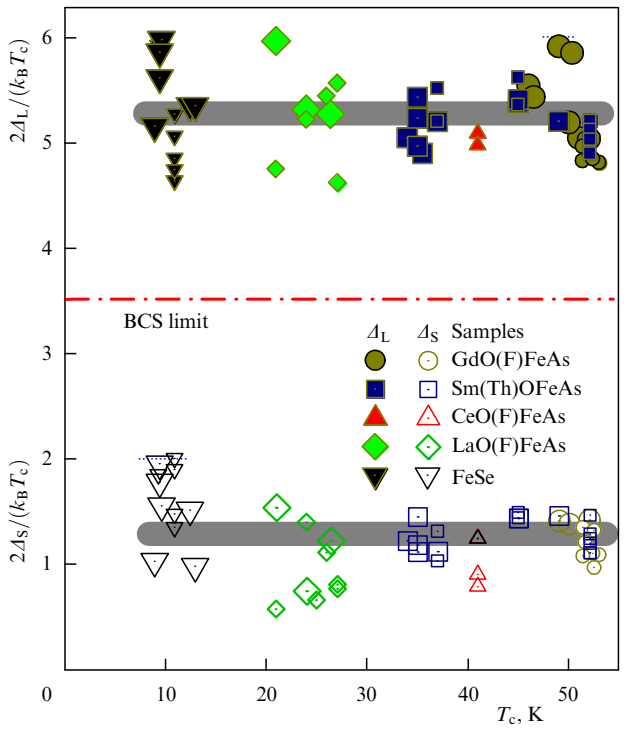

Figure 6. Dependence of the BCS ratio $2\Delta_i/(k_BT_c)$ for the large gap (solid symbols) and small gap (open symbols) on the critical temperature for Gd-1111 (circles), Sm-1111 (squares), Ce-1111 (up triangles), La-1111 (rhombs), and FeSe (down triangles). Large symbols depict the data corresponding to T_c^{local}, and small symbols show data corresponding to T_c^{bulk}. Solid guidelines fit the average BCS ratios, and the BCS limit is marked by the dashed–dotted line.

gaps remains constant within the range of these T_c. Averaging of the results in Fig. 5 leads to $\langle\Delta_L/\Delta_S\rangle \approx 4$. Notice that the magnitude of the order parameters obtained in both single-crystal and polycrystalline samples of FeSe are similar and belong to the same group (down triangles in Fig. 5).

The BCS ratios for each band are also unchanged within the uncertainty range (Fig. 6). For the large gap, the ratio is $2\Delta_L/(k_BT_c) = 4.6-6.0$, notably exceeding the weak-coupling BCS limit 3.52. This is probably caused by a strong electron–boson coupling in the bands with a large gap. The solid horizontal lines in Fig. 6 depict the average values of the BCS ratios. Obviously, there is no tendency to significant variation of the interaction strength (and, especially, of changing the coupling mechanism); the average value of the BCS ratio is $\langle 2\Delta_L/(k_BT_c)\rangle \approx 5.2$. A similar energy of magnetic resonance for oxypnictides, $E_{res}/(k_BT_c) = 5.1-5.3$, was obtained from polarized neutron scattering data in Refs [85, 86]. For the small gap, one has $2\Delta_S/(k_BT_c) = 0.6-2.0 \ll 3.52$. The obvious reason is that the observed common T_c is not the critical 'eigentemperature' of the small-gap condensate and does not describe its properties.

The eigenparameters of each superconducting condensate (in the hypothetical case of zero interband interaction), such as $2\Delta_L/(k_BT_c^L)$ and $2\Delta_S/(k_BT_c^S)$, together with the relative coupling constants (normalized to intraband λ_{LL} for the condensate with the large gap), the partial densities of states ratio $\alpha = \lambda_{LS}/\lambda_{SL} \equiv N_S/N_L$, and the ratio of effective intraband coupling to interband coupling, $\beta = [\lambda_{LL}\lambda_{SS}/(\lambda_{LS}\lambda_{SL})]^{1/2} = (V_{LL}V_{SS})^{1/2}/V_{LS}$, have been estimated from fitting the gap temperature dependences to the extended Moskalenko and Suhl model (see Table 1). Notably, all the $\Delta_{L,S}(T)$ dependences measured for different families look similar. For all the compounds studied, the eigenvalue $2\Delta_L/(k_BT_c^L)$ for the large gap condensate is about 4.2–4.8, and for the small gap condensate is, on average, somewhat less, varying from the BCS limit of 3.5 to 4.5. Superconductivity in both condensates, therefore, can be described in the framework of the strong-coupling Eliashberg theory [11].

Taking into account the presence of the strong isotope effect in iron-based superconductors [9] and some experimental data from Refs [19, 43], we conclude on a strong electron–phonon interaction *within each band*. The intraband interaction in the small gap bands is weaker: λ_{SS} accounts for, on average, 60% of λ_{LL}, which also supports the last conclusion. In spite of intraband interaction playing the key role in the superconductivity of oxypnictides ($\beta \gg 1$), when studying the two-gap state it is also necessary to take the interband interaction into account.

Our data demonstrate that the two condensates interact rather weakly (see Table 1), whereas it is due to $\lambda_{LS,SL} \neq 0$ that the small gap does not vanish at temperatures up to the local contact T_c^{local}; indeed, according to the theory [50–52] for zero interband coupling the small gap would close at its eigentemperature T_c^S. Therefore, superconductivity in the Δ_S-condensate at temperatures exceeding T_c^S is induced by the 'driving' Δ_L-condensate (i.e., due to the k-space proximity effect). This causes the large gap temperature dependence to bend down relative to the BCS-like function, leading to a 20–30% decrease in T_c^{local} with respect to the eigenvalue T_c^L (see Table 1). Since such sags are caused by the small gap band,

Table 1. Superconducting state parameters calculated by fitting the temperature dependences of the large gap and small gaps for La-, Sm-, and Gd-based oxypnictides.*

Parameters \ Compound	Gd-1111 [65]		La-1111	Sm-1111 [70]	
T_c^{local}, K	49	50	21	45	37
Δ_L, meV	12.5	11.2	5.4	10.5	8.3
Δ_S, meV	3	3	1.4	2.8	1,8
$2\Delta_L/(k_B T_c^{local})$	5.9	5.2	6	5.4	5.2
$2\Delta_S/(k_B T_c^{local})$	1.4	1.4	1.5	1.4	1.1
$2\Delta_L/(k_B T_c^{L})$	4.8	4.3	4.4	4.55	4.5
$2\Delta_S/(k_B T_c^{S})$	3.8	3.53	3.7	4.5	4.3
T_c^{local}/T_c^{L}	0.81	0.83	0.73	0.84	0.87
$\lambda_{SS}/\lambda_{LL}$	0.63	0.58	0.75	0.67	0.64
$\lambda_{LS}/\lambda_{LL}$	0.26	0.37	0.36	0.18	0.18
$\lambda_{SL}/\lambda_{LL}$	0.023	0.073	0.025	0.018	0.018
$\alpha = \lambda_{LS}/\lambda_{SL} = N_S/N_L$	11.2	5.1	15.5	10.3	9.7
$\beta = (V_{LL}V_{SS})^{1/2}/V_{LS}$	10.4	4.6	9.4	14.4	14

* $\lambda_{ij} = V_{ij}N_j$ are the electron–boson coupling constants, with $i = L, S$, and $j = L, S$.

their intensity should depend on the density of states ratio in two bands (the α parameter). We estimate the density of states in the small gap band to be an order of magnitude higher than that in the large gap band.

Thus, we have shown that the relative λ_{ij} and the BCS eigenratios $2\Delta_i/(k_B T_c^i)$ remain nearly constant under variations of both doping concentration and the constituting lanthanide Sm/Gd/Ce/La. The samples studied differ in the chemical compositions of the spacers rather than in the superconducting Fe–As blocks. The degree of structural ordering of the superconducting Fe–As blocks is nearly unchanged, whereas the doping level varies, leading to variations of the density of states $N_{L,S}$ in the bands.

Our studies thus prove the spacers in 1111 compounds to be charge reservoirs, and they are not involved directly in the superconductivity. The aforementioned variations of the chemical compositions are not supposed to affect the coupling mechanism or the strength of electron–boson interaction. In addition, taking into account the similar quasi-two-dimensionality of both condensates and the similarity of the Fermi surfaces for the 1111 family and FeSe [87], the experimentally observed scaling of both gaps with the critical temperature becomes obvious and agrees well with the available theory [24].

7. Conclusions

We studied iron-based superconductors of various families with critical temperatures covering almost all the range, from 9 K to maximal $T_c = 53$ K. In natural arrays of contacts formed in these materials, we observed intrinsic multiple Andreev reflections. The spectroscopy of such contacts demonstrated that the multiple Andreev reflections contribute significantly to transport along the *c*-direction in iron-based superconductors. In all compounds studied we detected two-gap superconductivity and determined the magnitude of the large and small superconducting gaps and the corresponding BCS ratios. The measured temperature dependences of the large and the small gaps $\Delta_{L,S}(T)$ are similar for various families of Fe-based superconductors and could be well fitted in the framework of the two-band Moskalenko and Suhl model. We conclude on the extended s-wave symmetry of the Δ_L order parameter (with an anisotropy of about 20–30% in the *k*-space) and on the absence of nodes for Δ_L.

Our studies revealed that the BCS ratio for bands with the large gap $2\Delta_L/(k_B T_c) \approx 5.2$ is nearly constant within the whole range of T_c (which means that the coupling strength is unchanged), reflecting approximately 20% reduction in T_c^{local} in relation to eigenvalue T_c^L, and the large gap roughly corresponds to the energy of magnetic resonance: $2\Delta_L \approx E_{res}$. This result requires special theoretical consideration.

Our estimates of the relative coupling constants and eigenparameters of each condensate (in the hypothetical case of a zero interband interaction), namely, $2\Delta_L/(k_B T_c^L) = 4.2-4.8$ and $2\Delta_S/(k_B T_c^S) = 3.5-4.5$ lead to the indirect conclusion that it is a strong electron–phonon interaction in each condensate described in the framework of the Eliashberg theory [11] that plays the key role in the superconductivity of iron-based oxypnictides. In this case, two condensates interact weakly with each other ($\beta \gg 1$; see Table 1). Nevertheless, in comparison with another two-gap superconductor, MgB_2, the interband interaction for the Fe-based compounds studied appears to be stronger, whereas the intraband interaction seems to be weaker. Indeed, for the σ-bands in MgB_2 the BCS eigenratio is about $2\Delta_\sigma/(k_B T_c^\sigma) \approx 5.1$ and $\beta = 10-20$ [88], while for the Ln-1111 family one has $\beta = 5-15$.

According to our data, the mean value of the gap ratio is about $\Delta_L/\Delta_S \approx 4$, being nearly constant within the whole range of $T_c = 9-53$ K. The observed scaling of superconducting gaps and T_c, as was discussed above, is caused by changing the density of states $N_{L,S}$ in the bands. According to the BCS theory, just increasing the intraband coupling constant $\lambda = VN$ enhances Δ and T_c. The ability of chemical doping to enhance the density of states N is very limited for the known iron-based superconductors. As regards the prospects of increasing V, we point to the hypothetical possibility of boosting the intraband coupling with an increase of the phonon density of states at high energies. The latter could be realized, for example, by a variation of crystal lattice parameters of iron-based superconductors or by an implantation of light atoms with the unfilled p-electron shell (B, C, N) to the periodic structure of the spacer layers.

Acknowledgments

The authors thank Yu F Eltsev, A V Sadakov, K S Pervakov, L F Kulikova, P I Arseev, N K Fedorov, D A Chareev, A N Vasiliev, O S Volkova, T Hänke, C Hess, G Behr, R Klingeler, B Büchner, and T Wolf. This research was supported by the Russian Foundation for Basic Research (project Nos 13-02-01451, and 14-02-90425).

References

1. Kamihara Y et al. *J. Am. Chem. Soc.* **128** 10012 (2006)
2. Sadovskii M V *Phys. Usp.* **51** 1201 (2008); *Usp. Fiz. Nauk* **178** 1243 (2008)
3. Ivanovskii A L *Phys. Usp.* **51** 1229 (2008); *Usp. Fiz. Nauk* **178** 1273 (2008)

4. Izyumov Yu A, Kurmaev E Z *Phys. Usp.* **51** 1261 (2008); *Usp. Fiz. Nauk* **178** 1307 (2008)
5. Abrikosov A A *Physica C* **317–318** 154 (1999)
6. Fujioka M et al., arXiv:1401.5611
7. Klauss H-H et al. *Phys. Rev. Lett.* **101** 077005 (2008)
8. Mazin I I, Schmalian J *Physica C* **469** 614 (2009)
9. Liu R H et al. *Nature* **459** 64 (2009)
10. Boeri L, Dolgov O V, Golubov A A *Physica C* **469** 628 (2009)
11. Eliashberg G M *Sov. Phys. JETP* **11** 696 (1960); *Zh. Eksp. Teor. Fiz.* **38** 966 (1960)
12. Mazin I I et al. *Phys. Rev. Lett.* **101** 057003 (2008)
13. Korshunov M M, Eremin I *Phys. Rev. B* **78** 140509(R) (2008)
14. de la Cruz C et al. *Nature* **453** 899 (2008)
15. Paglione J, Greene R L *Nature Phys.* **6** 645 (2010)
16. Onari S, Kontani H *Phys. Rev. Lett.* **103** 177001 (2009)
17. Efremov D V et al. *Phys. Rev. B* **84** 180512(R) (2011)
18. Sato M et al. *J. Phys. Soc. Jpn.* **79** 014710 (2010)
19. Ikeuchi K et al. *JPS Conf. Proc.* **3** 015043 (2014)
20. Ishizuka J et al. *J. Phys. Soc. Jpn.* **82** 123712 (2013)
21. Shein I R, Ivanovskii A L *Phys. Lett. A* **375** 1028 (2011)
22. Pandey S, Chubukov A V, Khodas M *Phys. Rev. B* **88** 224505 (2013)
23. Zhou Y et al., arXiv:1311.0611
24. Kuchinskii E Z, Nekrasov I A, Sadovskii M V *JETP Lett.* **91** 518 (2010); *Pis'ma Zh. Eksp. Teor. Fiz.* **91** 567 (2010)
25. Zhigadlo N D et al. *Phys. Rev. B* **86** 214509 (2012)
26. Malone L et al. *Phys. Rev. B* **79** 140501(R) (2009)
27. Hashimoto K et al. *Phys. Rev. Lett.* **102** 017002 (2009)
28. Prakash J et al. *J. Phys. Condens. Matter* **21** 175705 (2009)
29. Chen G F et al. *Phys. Rev. Lett.* **101** 057007 (2008)
30. Mu G et al. *Chinese Phys. Lett.* **25** 2221 (2008)
31. Nakai Y et al. *Phys. Rev. B* **79** 212506 (2009)
32. Kawasaki S et al. *Phys. Rev. B* **78** 220506(R) (2008)
33. Matano K et al. *Europhys. Lett.* **83** 57001 (2008)
34. Yin Y et al. *Physica C* **469** 535 (2009)
35. Kondo T et al. *Phys. Rev. Lett.* **101** 147003 (2008)
36. Sato T et al. *J. Phys. Soc. Jpn.* **77** 063708 (2008)
37. Sugimoto A et al. *Physica C* **470** 1070 (2010)
38. Ekino T et al. *Physica C* **470** S358 (2010)
39. Jin R et al. *Supercond. Sci. Technol.* **23** 054005 (2010)
40. Fasano Y et al. *Phys. Rev. Lett.* **105** 167005 (2010)
41. Millo O et al. *Phys. Rev. B* **78** 092505 (2008)
42. Miyakawa N et al. *J. Supercond. Novel Magn.* **23** 575 (2010)
43. Tanaka M, Shimada D *J. Supercond. Novel Magn.* **24** 1491 (2011)
44. Samuely P et al. *Supercond. Sci. Technol.* **22** 014003 (2009)
45. Le Tacon M et al. *Phys. Rev. B* **78** 140505(R) (2008)
46. Seidel P *Supercond. Sci. Technol.* **24** 043001 (2011)
47. Stewart G R *Rev. Mod. Phys.* **83** 1589 (2011)
48. Daghero D et al. *Supercond. Sci. Technol.* **25** 084012 (2012)
49. Daghero D et al. *Rep. Prog. Phys.* **74** 124509 (2011)
50. Moskalenko V A *Fiz. Met. Metalloved.* **8** 503 (1959)
51. Moskalenko V A *Sov. Phys. Usp.* **17** 450 (1974); *Usp. Fiz. Nauk* **113** 340 (1974)
52. Suhl H, Matthias B T, Walker L R *Phys. Rev. Lett.* **3** 552 (1959)
53. Andreev A F *Sov. Phys. JETP* **19** 1228 (1964); *Zh. Eksp. Teor. Fiz.* **48** 1823 (1964)
54. Abrikosov A A et al. *Phys. Usp.* **53** 103 (2010); *Usp. Fiz. Nauk* **180** 109 (2010)
55. Sharvin Yu V *Sov. Phys. JETP* **21** 655 (1965); *Zh. Eksp. Teor. Fiz.* **48** 984 (1965)
56. Octavio M et al. *Phys. Rev. B* **27** 6739 (1983)
57. Flensberg K, Hansen J B, Octavio M *Phys. Rev. B* **38** 8707 (1988)
58. Arnold G B *J. Low Temp. Phys.* **68** 1 (1987)
59. Kümmel R, Gunsenheimer U, Nicolsky R *Phys. Rev. B* **42** 3992 (1990)
60. Ponomarev Ya G et al. *JETP Lett.* **79** 484 (2004); *Pis'ma Zh. Eksp. Teor. Fiz.* **79** 597 (2004)
61. Kuzmichev S A et al. *Solid State Commun.* **152** 119 (2012)
62. Moreland J, Ekin J W *J. Appl. Phys.* **58** 3888 (1985)
63. Ponomarev Ya G et al. *Phys. Rev. B* **79** 224517 (2009)
64. Ponomarev Ya G et al. *JETP* **113** 459 (2011); *Zh. Eksp. Teor. Fiz.* **140** 527 (2011)
65. Shanygina T E et al. *JETP Lett.* **93** 94 (2011); *Pis'ma Zh. Eksp. Teor. Fiz.* **93** 95 (2011)
66. Pudalov V M et al. *Phys. Usp.* **54** 648 (2011); *Usp. Fiz. Nauk* **181** 672 (2011)
67. Shanygina T E et al. *J. Phys. Conf. Ser.* **391** 012138 (2012)
68. Kuzmichev S A et al. *JETP Lett.* **95** 537 (2012); *Pis'ma Zh. Eksp. Teor. Fiz.* **95** 604 (2012)
69. Shanygina T E et al. *J. Supercond. Novel Magn.* **26** 2661 (2013)
70. Ponomarev Ya G et al. *J. Supercond. Novel Magn.* **26** 2867 (2013)
71. Kuzmicheva T E et al. *Europhys. Lett.* **102** 67006 (2013)
72. Kuzmichev S A et al. *JETP Lett.* **98** 722 (2013); *Pis'ma Zh. Eksp. Teor. Fiz.* **98** 816 (2013)
73. Chareev D et al. *CrystEngComm* **15** 1989 (2013)
74. Kuzmicheva T E, Kuzmichev S A, Zhigadlo N D *JETP Lett.* **99** 136 (2014); *Pis'ma Zh. Eksp. Teor. Fiz.* **99** 154 (2014)
75. Roslova M et al. *CrystEngComm* **16** 6919 (2014)
76. Ponomarev Ya G et al. *Physica C* **243** 167 (1995)
77. Aminov B A et al., in *Advances in Superconductivity V* (Eds Y Bando et al.) (Tokyo: Springer-Verlag, 1993) p. 1037
78. Ponomarev Ya G et al. *Inst. Phys. Conf. Ser.* (167) 241 (2000)
79. Ponomarev Ya G *Phys. Usp.* **45** 649 (2002); *Usp. Fiz. Nauk* **172** 705 (2002)
80. Nakamura H et al. *J. Phys. Soc. Jpn.* **78** 123712 (2009)
81. Khlybov E P et al. *JETP Lett.* **90** 387 (2009); *Pis'ma Zh. Eksp. Teor. Fiz.* **90** 429 (2009)
82. Zhigadlo N D et al. *Phys. Rev. B* **82** 064517 (2010)
83. Kondrat A et al. *Eur. Phys. J. B* **70** 461 (2009)
84. Yanson I K et al. *Phys. Rev. B* **67** 024517 (2003)
85. Wakimoto S et al. *J. Phys. Soc. Jpn.* **79** 074715 (2010)
86. Shamoto S-I et al. *Phys. Rev. B* **82** 172508 (2010)
87. Subedi A et al. *Phys. Rev. B* **78** 134514 (2008)
88. Kuzmichev S A, Kuzmicheva T E, Tchesnokov S N *JETP Lett.* **99** 295 (2014); *Pis'ma Zh. Eksp. Teor. Fiz.* **99** 339 (2014)

PACS numbers: **74.25.–q, 74.45.+c, 74.70.–b**
DOI: 10.3367/UFNe.0184.201408j.0897

Magnetic and transport properties of single crystals of Fe-based superconductors of the 122 family

Yu F Eltsev, K S Pervakov, V A Vlasenko, S Yu Gavrilkin, E P Khlybov, V M Pudalov

1. Introduction

Iron-based superconductors, just after their discovery in 2008 [1–5], have become a subject of great interest for the scientific community and occupy one of the leading places among the most topical subjects in contemporary solid-state physics [6, 7]. The present development of investigations of iron-containing superconductors can be compared perhaps with the great efforts to study properties of cuprate high-temperature

Yu F Eltsev, S Yu Gavrilkin Lebedev Physical Institute, Russian Academy of Sciences, Moscow, Russian Federation
E-mail: eltsev@sci.lebedev.ru
K S Pervakov, V A Vlasenko Lebedev Physical Institute, Russian Academy of Sciences, Moscow, Russian Federation; International Laboratory for Strong Magnetic Fields and Low Temperatures, Wroclaw, Poland
E P Khlybov Vereshchagin Institute of High-Pressure Physics, Russian Academy of Sciences, Troitsk, Moscow, Russian Federation; International Laboratory for Strong Magnetic Fields and Low Temperatures, Wroclaw, Poland
V M Pudalov Lebedev Physical Institute, Russian Academy of Sciences, Moscow, Russian Federation; Moscow Institute of Physics and Technology, Dolgoprudnyi, Moscow region, Russian Federation

Uspekhi Fizicheskikh Nauk **184** (8) 897–902 (2014)
DOI: 10.3367/UFNr.0184.201408j.0897
Translated by S N Gorin; edited by A Radzig